Paleoceanography and Paleoclimatology

RESEARCH ARTICLE
10.1029/2025PA005316

chromatoPy: An Open-Source Tool for Chromatographic Peak Deconvolution and Integration Applied to Glycerol Dialkyl Glycerol Tetraethers

G. A. Otiniano[1], E. K. Thomas[1], I. S. Castañeda[2], S. Acharya[1], Y. Sharma[1], and S. Z. Mark[1]

[1]Department of Earth Sciences, SUNY, Buffalo, NY, USA, [2]University of Massachusetts Amherst, Amherst, MA, USA

Key Points:

- chromatoPy enables reproducible chromatographic peak integration using a multi-Gaussian fitting algorithm
- Peak areas calculated using chromatoPy are comparable to manual integration with low inter-user variance
- chromatoPy reduces processing time and introduces uncertainty quantification of calculated peak areas

Supporting Information:

Supporting Information may be found in the online version of this article.

Correspondence to:

G. A. Otiniano,
gerardotiniano@gmail.com

Citation:

Otiniano, G. A., Thomas, E. K., Castañeda, I. S., Acharya, S., Sharma, Y., & Mark, S. Z. (2025). chromatoPy: An open-source tool for chromatographic peak deconvolution and integration applied to glycerol dialkyl glycerol tetraethers. *Paleoceanography and Paleoclimatology*, *40*, e2025PA005316. https://doi.org/10.1029/2025PA005316

Received 4 SEP 2025
Accepted 24 NOV 2025

Author Contributions:

Conceptualization: G. A. Otiniano, E. K. Thomas, S. Z. Mark
Data curation: I. S. Castañeda
Formal analysis: G. A. Otiniano
Funding acquisition: E. K. Thomas
Investigation: G. A. Otiniano
Methodology: G. A. Otiniano, E. K. Thomas, I. S. Castañeda, S. Z. Mark
Software: G. A. Otiniano, Y. Sharma
Validation: G. A. Otiniano, S. Acharya
Visualization: G. A. Otiniano
Writing – original draft: G. A. Otiniano
Writing – review & editing: E. K. Thomas, I. S. Castañeda, S. Acharya, S. Z. Mark

Abstract Glycerol dialkyl glycerol tetraethers (GDGTs) are valuable proxies for reconstructing past environmental conditions but sources of analytical uncertainty remain unresolved, as highlighted by a recent inter-laboratory comparison project. Analytical uncertainties owe in part to subjective solutions to manual peak integration, including baseline corrections, peak deconvolution, and signal smoothing. Here, we present chromatoPy, an open-source Python package implementing a multi-Gaussian fitting algorithm that automatically models peak co-elution while requiring user approval of the fitted results, thereby improving peak area integration accuracy, enhancing reproducibility, and reducing the time required for peak processing. We evaluate chromatoPy through inter-user comparisons and against manual integration using a global data set of GDGTs from marine, lacustrine, and loess sediments, demonstrating high concordance in peak areas and fractional abundances for both branched and isoprenoid GDGTs. Subtle but systematic differences are observed primarily for branched GDGTs prone to co-elution, which is consistent with the deconvolution approach employed. By reducing analyst subjectivity and providing uncertainty estimates, chromatoPy facilitates more comparable GDGT measurements across laboratories and data sets, thereby strengthening the foundations of GDGT-based paleoclimate and biogeochemical reconstructions. The package significantly decreases processing time while providing quantitative uncertainty estimates using Monte Carlo error propagation, enabling rapid replicate analyses. chromatoPy thus offers a robust, user-friendly tool that enhances reproducibility and will ultimately yield more reliable paleoclimate reconstructions.

1. Introduction

Glycerol dialkyl glycerol tetraethers (GDGTs) have become increasingly popular proxies for reconstructing paleoenvironmental conditions. This popularity owes to their ability to record multiple environmental parameters (e.g., temperature, pH, conductivity; Raberg et al., 2021) during synthesis by a diverse and incompletely characterized suite of microbes (e.g., Chen et al., 2022; Sinninghe Damsté et al., 2011; Weijers et al., 2006; Zeng et al., 2022). Additionally, the ubiquity (e.g., Raberg et al., 2022) and persistence (e.g., Naafs et al., 2018; Otiniano et al., 2020) of GDGTs in the geological record ensure broad spatial and temporal applicability, making them exceptionally valuable for climate reconstructions.

The methods for GDGT extraction from environmental matrices are well established, and since their initial identification, advancements in High Pressure Liquid Chromatography Mass Spectrometry (HPLC-MS) have improved the analytical procedures for measuring these compounds (e.g., Becker et al., 2015; De Jonge et al., 2013; Hopmans et al., 2016; Rattray & Smittenberg, 2020). However, a comparison of GDGT compound quantification between 44 laboratories found discrepancies in the final compound concentrations, with replicate measurements of branched and isoprenoid GDGTs exhibiting standard deviations ranging from 61% to 105% of the mean concentration values (De Jonge et al., 2024). These results indicate substantial interlaboratory variance, owing in part to differences in peak integration practices (De Jonge et al., 2024). Indeed, the application and method for correcting baseline shifts in HPLC-MS data, determining the extent of peak tails, and integrating co-eluting peaks are not standardized practices and are likely causes of variability between laboratory groups and individual researchers (De Jonge et al., 2024).

Here, we introduce a software package, chromatoPy, which offers a user-friendly environment where researchers can pre-process, visualize, and integrate HPLC-MS chromatography data, and output results. In contrast to proprietary software for chromatography, chromatoPy is open-source, promoting reproducibility and collaboration for researchers currently, or interested in, analyzing GDGTs. We evaluate the performance and

reproducibility of chromatoPy for the quantitative analysis of GDGTs. Specifically, we test the reliability of chromatoPy through inter-user comparisons and against manually integrated data sets, assessing agreement in peak areas, fractional abundances, and a commonly used temperature proxy (MBT'_{5Me}). These comparisons allow us to determine whether chromatoPy produces results consistent with expert manual integration while also revealing potential systematic differences that may arise from the Gaussian deconvolution framework. Additionally, we assess the quantitative uncertainty estimates generated by chromatoPy to evaluate how well the modeled peaks fit the observed signal and to determine whether uncertainty can thus as a diagnostic indicator of potential challenges in peak integration or chromatographic quality. Together, these analyses establish a foundation for transparent, reproducible, and quantitively robust GDGT data processing.

2. Methods and Materials

High Pressure Liquid Chromatography Mass Spectrometry analysis of GDGTs produces chromatograms in which each trace corresponds to an ion mass-to-charge ratio (m/z) and records ion intensity as a function of retention time. These multidimensional data are typically exported from instrument-specific software in proprietary binary formats that require conversion before further processing. ChromatoPy operates downstream of this step, providing a semi-automated framework for chromatographic peak identification, deconvolution, and integration (Figure 1).

As a general overview of the workflow (Figure 1), the user first provides chromatoPy with the raw chromatographic data as comma-separated value (CSV) files and select the GDGT classes to be analyzed. The software applies baseline and retention-time corrections across all samples and then displays chromatograms for the first sample. The user selects the peaks of interest in this first sample and the corresponding retention times are then stored as references for chromatoPy to identify and integrate peaks in subsequent samples. This workflow enables efficient and consistent processing across large data sets while preserving user oversight to verify automatic peak selections and identify potential chromatographic or analytical issues.

We wrote chromatoPy in Python, using a number of readily available packages (Table 1). ChromatoPy reads chromatography data formatted as CSV files that follow a specific column structure and header convention. In its current configuration, this format is derived from Agilent's ChemStation output processed through the open-source package rainbow (https://github.com/evanyeyeye/rainbow). A wrapper of rainbow is included within chromatoPy as an optional preprocessing tool to facilitate conversion of ChemStation binary files to the required CSV structure. Although we cannot guarantee compatibility with data exported from other HPLC software platforms without additional preprocessing or modification, chromatoPy can process raw HPLC data from any instrument provided that the data are exported or reformatted to match the expected CSV layout. Users may generate such CSVs directly from their own acquisition software or employ conversion tools such as rainbow. The raw data used in this study are archived on Zenodo (Otiniano et al., 2025) and serve as examples of the required format for preparing and verifying users.

2.1. GDGT Testing Data Set

To assess the accuracy of chromatoPy's peak integration, we processed the raw data of 84 samples previously analyzed for GDGTs using proprietary software, Agilent's ChemStation (Table 2). Lipid extraction and GDGT quantification methods were consistent across sample sets following the procedure described in Schneider et al. (2024). The GDGTs were originally measured at UMass using an Agilent 1,260 High-Performance Liquid Chromatograph coupled to an Agilent 6,120 Quadrupole Mass Spectrometer following the analytical method outlined by Hopmans et al. (2016). These samples represent a range of environments, from tropical to polar, and reflect sites that differ substantially in GDGT distributions (e.g., branched vs. isoprenoid dominated) and concentrations (Table 2). We also compare the two methods on a timeseries record using a sediment core from Lake Bolshoye Shchuchye, Russia, which spans the past 24 kyr ($n = 55$) (Haflidason et al., 2022). The majority of samples were analyzed for brGDGTs (15 unique structures) and isoGDGTs (6 unique structures) with the exception of six samples, in which only isoGDGTs were processed, yielding 1,668 potentially identifiable peaks (Table 2). We did not assess performance on hydroxylated isoprenoid GDGTs (OH-GDGTs) or glycerol monoalkyl glycerol tetraethers (GMGTs).

Importantly, ChemStation and chromatoPy process data using different time units (minutes and seconds, respectively), resulting in area units that are not directly comparable. We therefore implement two scaling techniques to compare between integration methods. The first technique ("Scaled Peak Area") scales all peaks to the

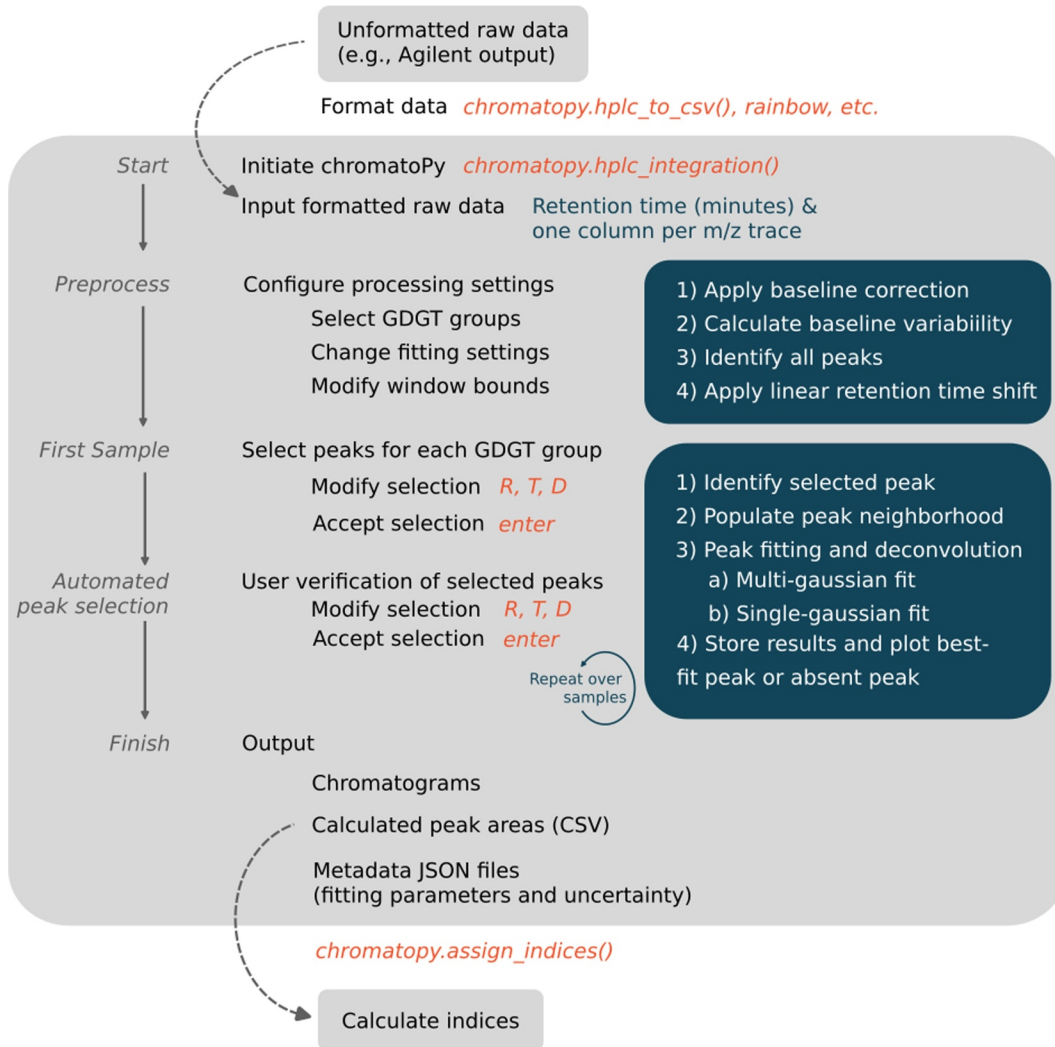

Figure 1. Overview of the chromatoPy workflow. Workflow steps (gray, italicized) are shown with their associated commands (orange, italicized). Fundamental steps are connected by solid arrows, while optional steps are indicated by dashed arrows. Algorithmic processes (white) are summarized at the locations corresponding to where they occur in the workflow.

largest peak area observed across all GDGTs and samples for each method independently. This scaling preserves relative differences in area within each method while allowing comparison on common scale across methods. We divide the peak area of each GDGT by the largest peak area observed across all samples, for each integration method separately. The second technique independently calculates fractional abundances of GDGTs from the original (unscaled) peak areas, expressed relative to total isoprenoid (iso) or total branched (br) GDGT within each sample, which is the typical format for reporting GDGT data. For this study, we target isoGDGTs GDGT-0, GDGT-1, GDGT-2, GDGT-3, GDGT-4, and GDGT-4′ as well as brGDGTs Ia, IIa, IIIa, IIa′, IIIa′, Ib, IIb, IIIb, IIb′, IIIb′, Ic, IIc, IIIc, IIc′, and IIIc′.

Table 1
Python Packages and Version Numbers Used in chromatoPy

Package	Version
Numpy	1.26.4
Pandas	2.2.2
Scikit-learn	1.4.2
SciPy	1.13.1
Matplotlib	3.8.4
Rainbow	2.8.0
Pybaselines	1.1.0

2.2. Development

One of the challenges in automating the identification and processing of compounds measured via HPLC-MS analysis (e.g., Hopmans et al., 2016) is the non-stationarity of retention times. Retention times can vary as a result of

Table 2
Summary of Sample Locations, Sediment Types, Age, Number of Samples, and Glycerol Dialkyl Glycerol Tetraether Types Analyzed in the Testing Data Set

Site	Location	Age	Sediment type	Sample count	GDGT type
Lake Issyk-Kul	Kyrgyzstan	Modern	lacustrine	4	br-, isoGDGTs
Lake El'gygytgyn,	Siberia	Modern	lacustrine	3	br-, isoGDGTs
–	Croatia	Modern	lacustrine	3	br-, isoGDGTs
Lake Malawi	Mozambique	Modern	lacustrine	4	br-, isoGDGTs
Lake Bolshoye Shchuchye	Siberia	Modern to 24 kyr cal BP (Haflidason et al., 2022)	lacustrine	55	br-, isoGDGTs
–	Offshore of Northwest Africa	Modern	marine	3	br-, isoGDGTs
–	Offshore of Northwest Australia	Modern	marine	2	br-, isoGDGTs
–	Offshore of New Jersey	Modern	marine	1	br-, isoGDGTs
ODP Site 846	–	Miocene	marine	3	isoGDGTs
ODP Site U1450	–	Pliocene and Pleistocene	marine	3	isoGDGTs
–	Alaska	Pleusticene	loess	3	br-, isoGDGTs

fluctuations in experimental conditions including but not limited to column temperature, mobile phase composition, flow rate, and column conditions, which affect the interaction between analytes and the stationary phase, leading to changes in elution time. ChromatoPy attempts to automatically detect this variability by identifying a shared reference peak in every sample. Assuming the samples were analyzed with a C_{46} glycerol trialkyl glycerol tetraether internal standard (Huguet et al., 2006; Patwardhan & Thompson, 1999), the reference peak of this standard (identified with a mass to-charge ratio of 744) is used to apply a linear shift correction to the retention time of each sample. Users may also specify an alternative GDGT of high prominence (e.g., GDGT-0) that is consistently present across their data set. The accuracy of the retention-time correction was verified by comparing the reference-standard peaks identified by chromatoPy against the original chromatograms.

2.2.1. Signal Processing

To reduce noise and emphasize peak structures in the raw HPLC-MS data, we employ a smoothing algorithm. We implement a Savitzky-Golay filter, a least squares polynomial fitting function (Savitzky & Golay, 1964) with a default filter window of 12 data points, typically reflecting 14.7 s of data collection, and a third-order polynomial. The Savitzky-Golay filter is an optimal smoothing function as it is computationally efficient and preserves signal-to-noise ratios (Savitzky & Golay, 1964). It is important to acknowledge that the filter can introduce artifacts at the margins of the data range (Schmid et al., 2022); however, given the 12-point window and corresponding time span, only the initial and final ∼7.4 s of the record are affected by these edge artifacts.

To correct for baseline shifts in the chromatography signal, we follow a similar approach to that of (Mecozzi, 2014). We approximate the baseline using an iterative polynomial fitting function with a default order of 5 and convergence tolerance of 10^{-4} (Equation 1)

$$B(x) = a_5x^5 + a_4x^4 + a_3x^3 + a_2x^2 + a_1x^1 + a_0 \quad (1)$$

where B(x) is the baseline function, a_n denotes the nth coefficient, and x refers to the retention time. The coefficient vector is determined by an iterative least-squares fitting procedure. In each iteration k, the coefficients are updated via Equation 2

$$a^{k+1} = V^{+}y^{k} \quad (2)$$

where V^{+} denotes the pseudo-inverse of the Vandermonde matrix constructed from the x-values and y^k is the signal at iteration k. After computing B(x) with updated coefficients, the signal is modified by taking the element-wise minimum. The iterative process terminates when the relative change in the coefficient vector is below the default tolerance, 10^{-4}.

To identify peaks in the signal, we use the function find_peaks from the package Scipy (Virtanen et al., 2020). This function is effective as parameters of peak amplitude, width, and prominence can be used to filter for specific conditions (Virtanen et al., 2020). For example, we use the minimum peak height argument to filter for peaks too small for confident integration. Here, the minimum threshold is defined as three times the baseline variability (Currie, 1995). We calculate baseline variability by filtering for regions of the baseline-corrected signal without peaks using the package pybaselines (Erb, 2024), calculating the standard deviation of this region, and then multiplying the standard deviation by three. If a peak exceeds this threshold in the composite signal but falls below it after deconvolution, chromatoPy treats the peak as absent.

2.2.2. Peak Fitting and Uncertainty

To identify the peak shape and ultimately calculate the area under the peak, we use a Gaussian fitting model similar to (Fleming & Tierney, 2016). Gaussian fitting is achieved by first estimating initial Gaussian parameters from the peak height, the width of the peak at 50% amplitude, and the retention time of the peak in the smoothed, baseline-corrected signal. We then iteratively modify these parameters to find the optimized fit via the Gaussian equation (Equation 3)

$$y = \text{amplitude} \times e^{-\frac{(x-\text{center})^2}{2\times\text{width}^2}} \quad (3)$$

where x is the retention time, y is the signal strength at x, center is the retention time at the middle of the peak, amplitude is the signal strength at center (i.e., the maximum signal strength), and width is the span of time at half maximum of the peak. The optimal peak-fit is determined using curve_fit from the Scipy package with 4,000 iterations to achieve convergence. We define the peak boundaries where the first derivative on either side of the peak is 0.1.

During peak fitting, we also calculate uncertainty associated with the iterative peak fitting process using Monte Carlo error propagation (e.g., Anderson, 1976), by quantifying the variability of the fitted Gaussian parameters. The curve_fit function operates similarly to the iterative polynomial fitting function (Section 2.2.1), outputting a set of optimized parameters for the fitted equation and the covariance matrix used to derive these fitted values. Opportunely, the uncertainty associated with the fitted parameters can be inferred from this covariance matrix by calculating the standard deviation of the diagonal, yielding a confidence metric. ChromatoPy uses this uncertainty to calculate an ensemble of signals and then integrates these synthetic signals using Scipy's Simpson function, an integration of a signal y(x) along a range of x using Simpson's rule (Virtanen et al., 2020). Once a sample has been processed, chromatoPy exports a JavaScript Object Notation file containing the peak fitting parameters and associated uncertainty terms for each peak selected in the sample. The structure and contents of these files are described in Text S1 in Supporting Information S1. Our novel incorporation of peak-fit uncertainty is important for subsequent data comparisons between samples and may ultimately improve uncertainty quantification of environmental inferences from GDGTs.

2.2.3. Peak Deconvolution

The process of peak fitting must also address the challenge of co-eluting peaks, which often arises from distinct compounds with similar masses—such as isomers—that are difficult to separate via column chromatography. This issue is especially pronounced for GDGTs, where high molecular masses and subtle structural differences arising from the positions of methylations and cyclopentane moieties (e.g., De Jonge et al., 2013; Schouten et al., 2002, 2007) complicate isomer separation. For GDGT quantitation, typical efforts to identify and calculate the area under these curves involve declaring strict boundaries for the peaks that yield truncated peak areas. Meanwhile, alternative approaches, such as fitting Gaussian distributions to the signal, do not consider the additive effect of overlapping peaks, resulting in potentially overestimated peak areas (Fleming & Tierney, 2016).

We implement a multi-Gaussian model to account for peak co-elution. Multi-Gaussian modeling is a robust method for the deconvolution of peaks in chromatography data (e.g., Felinger, 1994; Johansson et al., 1993). Subsequent studies have augmented this approach by incorporating more complex Gaussian mixing models and distribution shapes to improve signal fitting (e.g., Vemula et al., 2017; Wei et al., 2014; Yu & Peng, 2010). However, these approaches are, in comparison, computationally expensive. Here, we simplify the approach by targeting GDGT quantitation from HPLC-MS analysis in tandem with two assumptions. First, we assume that

Table 3
User Keys and Descriptions of Subsequent Actions Available to the User in chromatoPy

Hotkey	Description
up/down	Select peak or place peak place-holder
D	Delete last selected peak or place-holder
R	Delete all selected peaks and place-holders in a trace subplot
T	Delete all selected peaks and place-holders across all traces and assigns current sample as the new reference
W	Displays editable window boundaries

each peak follows a Gaussian distribution, as has been previously assumed for Gas Chromatograph and HPLC-MS data (Fleming & Tierney, 2016). Second, we assume that co-eluting peaks are individually identifiable, requiring that the maximum amplitudes of some pair of peaks are separated by a local minimum.

To deconvolve co-eluting peaks, chromatoPy first defines a peak neighborhood, that is, a set of peaks whose boundaries overlap. A composite model is constructed as the sum of individual Gaussian functions, each with its own initial parameter estimates. This multi-Gaussian model is then iteratively optimized, using curve_fit, to capture incremental changes in the root mean square error (RMSE) between the composite model and the original signal. The fitting routine is repeated for every combination of overlapping peaks by progressively removing the farthest peak from the peak of interest, ensuring that all potential configurations are considered. The fitting parameters for the selected peak are then extracted from the covariance of the multi-Gaussian model and used to calculate the peak area and associated uncertainty as explained in Section 2.2.2.

2.3. Implementation

When running chromatoPy, the user is first prompted for the type—or group of types—of GDGT data to be analyzed (e.g., brGDGT and isoGDGT). Next, the user is prompted for the file locations of the raw data. Once provided, the program creates an output folder in the same directory and loads the first chromatogram for processing.

The first figure of each sample displays the internal standard. The user then identifies the peak of interest by clicking near the peak; the identified peak area turns gray. For traces with several expected peaks, chromatoPy relies on relative retention times to assign labels. In scenarios where a peak is absent from the chromatogram, the user must click on its expected location, which will be marked by a vertical dashed-line placeholder. The user can advance to the next GDGT subset figure, or sample, using the enter key (Table 3).

The peak retention times recorded for each user-selected GDGT in the first sample are stored as reference values, enabling automatic peak identification in all subsequent samples. The user must view the peak integration for each sample and accept these automatically identified peaks using the enter key, which also advances to the next GDGT subset or sample. To update the reference retention times for all selected peaks in a current figure and all subsequent samples, the user can use the *T* key, which will remove all automatically selected peaks. The user can then select new peaks, which will be updated for the current GDGT subset and the rest of the samples in the sequence. Alternatively, the user can scroll through the trace panels using the up and down keys and delete automatically selected peaks in a given panel using the *R* key. This does not update selections for subsequent samples. Finally, the user can also delete the last selected peak or place holder using the *D* key. Importantly, reference peak times are only updated when using the *T* key.

After each sample is processed, either by the user or automatically, chromatoPy saves the calculated peak area (in units of amplitude•min) results to a CSV file and images of the integrated chromatograms as PNG files in the subfolder created within the output folder. This means that a user can exit the program after completing a sample without losing progress. Moreover, a sample can be reanalyzed by deleting the associated row from the CSV file and rerunning the sample. Once complete, the user can run the function calculate_indices, which produces three outputs: a CSV file containing the fractional abundances of GDGTs grouped by GDGT type, a CSV file containing the fractional abundances of brGDGT methyl- and cyclic-group sets, as defined by (Raberg et al., 2021), and a CSV file containing the calculated indices (Table 4).

Table 4
Indices and Associated References That Are Automatically Calculated Using chromatoPy

Index	Reference
MBT'_{5Me}	De Jonge et al. (2014)
CBT_{5Me}	De Jonge et al. (2014)
CBT′	De Jonge et al. (2014)
IR_{6Me}	De Jonge et al. (2014)
DC	Baxter et al. (2019)
Cald/Cren	Zhang et al. (2016)
HP5	Yao et al. (2020)
BIT	Hopmans et al. (2004)
fC	Martínez-Sosa and Tierney (2019)
Methylation set	Raberg et al. (2021)
Cyclization set	Raberg et al. (2021)

3. Validation

3.1. Peak Identification

Of the possible 1,668 potentially identifiable peaks, chromatoPy and the manual integration method commonly identified the presence or absence of 1,596 peaks (95.7%) (Figures 2a and 2b). ChromatoPy identified 16 peaks that were not identified manually, reflecting minor, user-specific differences in time-dependent GDGT selection. Conversely, the manual workflow reported 62 peaks that chromatoPy rejected. Approximately half of these peaks ($n = 33$) fell below chromatoPy's minimum amplitude threshold. These 33 peaks were predominantly GDGT-3, GDGT-4′, IIc′, IIIb′, and IIIc′, which are generally characterized by low abundance. The remaining 29 peaks did not have a distinguishable minimum between adjacent maxima, and therefore could not be separated by the multi-Gaussian algorithm.

Two important insights can be drawn from this analysis. First, while the chromatoPy minimum peak threshold successfully excludes low-signal noise, the threshold may cause expert-identified peaks to be omitted. Second, co-elution where peaks are not adequately separated to yield a measurable minimum remains a blind spot to chromatoPy's algorithm, even though manual integration may separate the peaks. The peak amplitude and co-elution scenarios introduce subjectivity into manual GDGT integration, as the decision to integrate or discard challenging peaks will vary between analysts, a potential source of uncertainty in GDGT integration (e.g., De Jonge et al., 2024). By contrast, chromatoPy provides a conservative, fully quantitative approach that applies a consistent, transparent threshold to these scenarios. This not only enhances reproducibility, reducing intra- and inter-user variability, but also aligns with the best practices suggesting that true co-elution often requires instrumental re-analysis for un-ambiguous resolution (Fleming & Tierney, 2016).

The following sections focus on the 1,596 peaks recognized by both methods, allowing direct comparison of integrated Scaled Peak Areas, Fractional Abundances, and associated uncertainties.

3.2. Inter-User Comparison

To determine the potential influence of user decisions on peak areas integrated using chromatoPy, a second user independently processed the full data set without any prior knowledge of the initial selection process. Considering the 1,596 peaks, the associated peak areas (Figure 2c, Figure S1 in Supporting Information S1) and fractional abundances (Figure 2d) independently calculated using chromatoPy are effectively identical, yielding Pearson's correlation coefficients greater than 0.999 ($p < 0.001$) and equal to 0.998 ($p < 0.001$), respectively. Moreover, the median percent difference between replicate analysis was low at 0.020% (1-σ range: −0.486% to 1.58%). Importantly, 8 brGDGT peaks and 1 isoGDGT peak, in a total of 9 samples, were assigned differently by the two users (11% of samples analyzed, 0.01% of all peaks identified) (Figures 2c and 2d). Excluding all other peaks from samples containing these discordant assignments, given their impact on fractional abundance for all peaks in a sample, the correlation coefficients for both peak area and fractional abundance are greater than 0.999, with a median percent difference of 0.022% (1-σ: −0.457%—1.590%). This consistency underscores the robustness of chromatoPy in generating reproducible peak area measurements.

Residual analysis of the chromatoPy peak area calculations by two different users (Figure 3a–3c) reveals relatively minor but important differences that guide definition of a practical minimum area threshold for reliable peak integration by chromatoPy. In general, the relative difference in calculated peak areas between users (hereafter "replicate difference") is inversely proportional to peak area size (Figures 3a and 3b), indicating greater reproducibility for larger peaks. A threshold of approximately 400 amplitude•minutes best separates the variance in replicate differences. Below this threshold, the median percent difference in peaks is 0.6% with a 95% range from −15.1% to 17.7%, while for peaks above the threshold the median is 0.7% with a tighter 95% range from −2.0% to 10.0%. Similarly, replicate differences were more frequently explained by the 1-σ peak area uncertainties for larger peaks (89%) compared to smaller peaks (85%). Together, these results demonstrate that, in general, replicate discrepancies in larger peaks are consistent with expected uncertainty (i.e., uncertainty associated with peak area integration), while smaller peaks carry more unexplained variance.

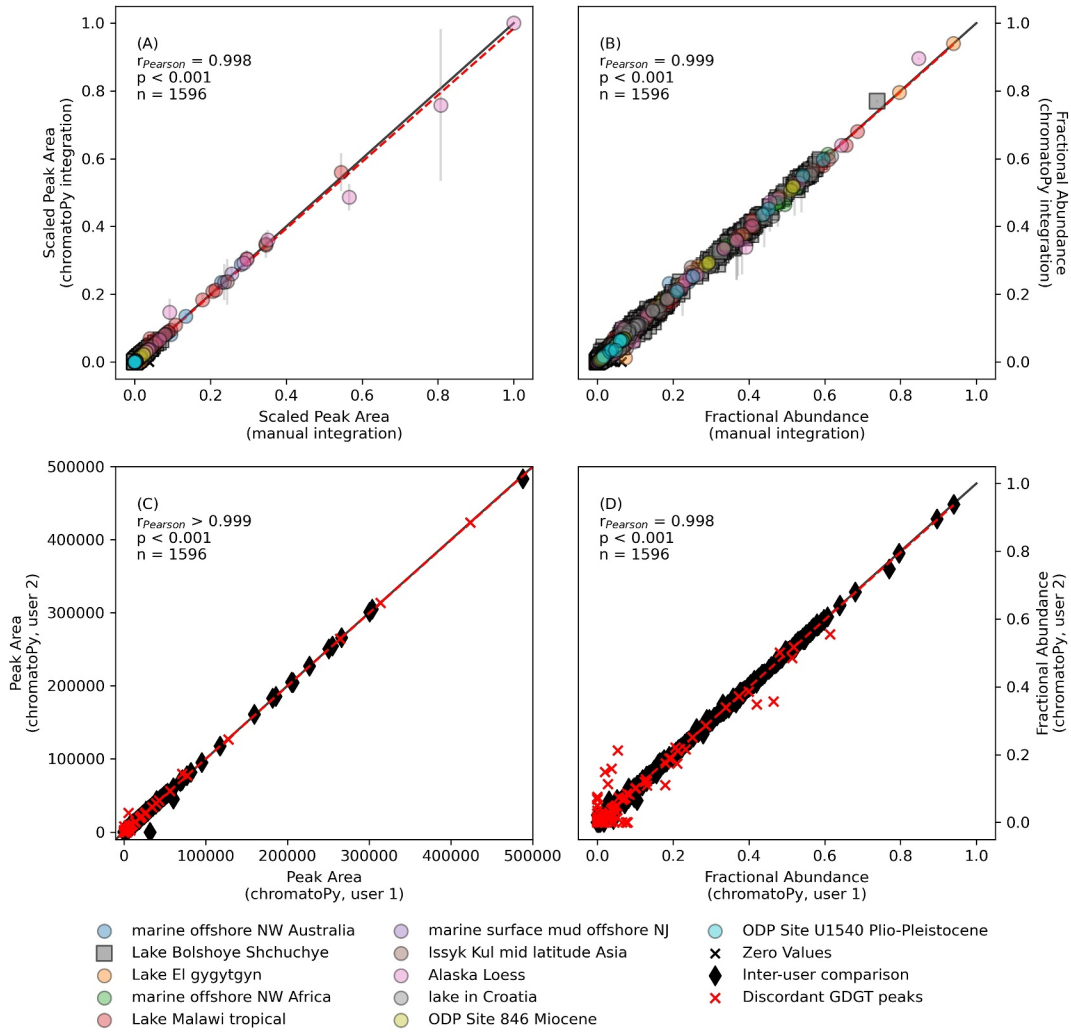

Figure 2. Comparison of chromatoPy and manual integration methods by (a) scaling peak areas to the maximum value observed across all samples, and (b) the fractional abundance of Glycerol dialkyl glycerol tetraethers (GDGTs) in each sample. Gray lines indicate propagated uncertainty for individual peaks calculated using chromatoPy. (c) Peak areas independently integrated by two users using chromatoPy. (d) Associated fractional abundances of GDGTs from each user's integration. Red x's highlight samples where users identified different peaks for one or more GDGTs ($n = 9$ peaks in 9 samples), resulting in discrepancies in fractional abundances.

In practice, peaks below the 400 amplitude•minute threshold can be quantified, but should be interpreted with caution as their replicate reproducibility is less certain. Although their median percent difference is relatively small (0.7%), additional replication, such as multiple users independently processing the data, can provide a more reliable assessment of user-dependent variability. Opportunely, chromatoPy greatly reduces the time requirement for processing samples. Manual peak integration can take upwards of 20 to 30 minutes per sample when processing both br- and isoGDGTs, with processing times increasing further when OH-GDGTs and GMGTs are included. In comparison, per-sample processing times using chromatoPy are an order of magnitude smaller, albeit subject to computer resource availability. For reference, we ran chromatoPy on a 2022 Macbook Air equipped with a M2 processor and 24 Gb of RAM.

Overall, chromatoPy facilitates reproducible peak area integration with minimal variability introduced by user decisions. Differences in peak identification between users could be alleviated by measuring a sediment standard with well resolved GDGT peaks at the beginning of each sequence and using that to set the peak timing when beginning the peak integration in chromatoPy. Moreover, by significantly reducing analysis time, potentially

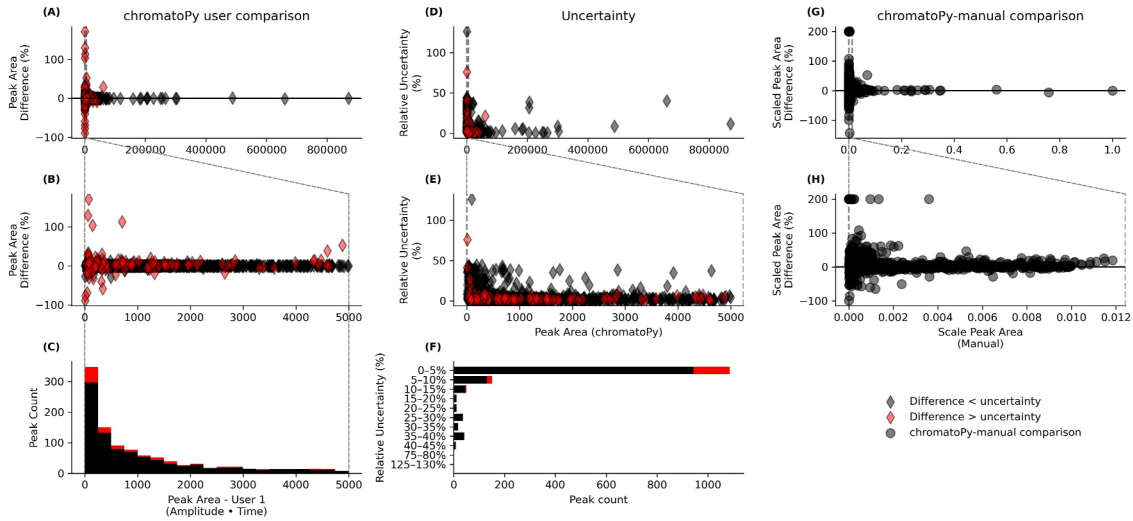

Figure 3. Validation metrics of peak integration. Left column illustrates inter-user comparisons of peak areas calculated using chromatoPy. Percent differences in peak areas are shown for (a) all detected peaks and (b) peaks with areas smaller than 5,000 amplitude•minutes. Data points are displayed as diamonds, color-coded based on whether the 1-σ uncertainty is less (black) or greater (red) than the difference in replicate measurements. (c) Histogram displaying the number of peaks within each category, organized into 250 amplitude•minute-wide bins (same color scheme as A–B). Center column depicts relative uncertainty (uncertainty divided by peak area) in peak area measurements for all peaks (d) and peaks with areas less than 5,000 amplitude•minutes (e). Histogram of relative peak area uncertainties (binned in 5% intervals), excluding bins with zero counts (f). Color coding carries over from panels A–C, with black and red reflecting peaks with 1-σ uncertainties less than (black) or greater than (red) the difference in replicate integrations by multiple users. Right column compares scaled peak areas calculated manually and using chromatoPy. (g) Percent differences of scaled peak areas are shown for all peaks and (h) peaks with a scaled area below 0.01.

unconstrained sources of uncertainty can be quantified via rapid replicate analyses and incorporated into the parameter uncertainty (Section 3.4).

3.3. Peak Area and Fractional Abundance Comparison

In general, peak areas calculated using chromatoPy yield similar results to those manually integrated in ChemStation. Considering the scaled peak areas and fractional abundances of all GDGT structures (Figures 1a and 1b; 2 F, G) the two methods yield a Pearson's correlation coefficient greater of 0.998 ($p < 0.001$), and 0.999, respectively, indicating that chromatoPy offers comparable peak measurements to manual integration. Importantly, the agreement of the calculated peak area does not decay when considering smaller peaks. For example, when considering individual GDGT types, lower-abundance GDGTs (e.g., IIIc and IIIc′) yield similar correlation statistics to higher-abundance GDGTs (e.g., Ia, GDGT-4; Figure 4).

The similarity between scaled peak areas derived from manual integration and ChromatoPy is further supported by a Wilcoxon signed-rank test for differences between median values. For the fractional abundance of all isoGDGTs, no significant difference was detected ($p = 0.84$). Significant differences were observed for the scaled peak areas of isoGDGTs and the scaled peak areas and fractional abundances of brGDGTs ($p < 0.001$), but the median differences were negligible (-8.3×10^{-6}, -2.3×10^{-5}, and 2.1×10^{-4}, respectively).

When considering individual GDGT types, most show comparable scaled peak areas and fractional abundances between the two methods (Figure 3). The differences in tetramethylated brGDGTs and isoGDGTs are either not significant or can be explained by uncertainty, indicating no systematic difference in peaks size (Table 5, Table S1 in Supporting Information S1). This is consistent with the expected performance of chromatoPy's peak fitting algorithm, as these compounds are generally less affected by co-elution. Importantly, this suggests that ChromatoPy's preprocessing steps do not introduce substantial biases into the ultimate peak area estimation.

By contrast, the fractional abundances and scaled peak areas of the 5- and 6-methyl penta- and hexa-methylated brGDGTs, display systematic differences that cannot be explained by uncertainty alone (Table 5, Table S1 in Supporting Information S1). Specifically, ChromatoPy tends to assign smaller areas to the 5-methyl brGDGTs and larger areas to the 6-methyl brGDGTs, which are typically smaller. A similar pattern is observed for the IIIa and IIIa′ peaks, though in those cases the differences largely fall within uncertainty. This behavior is consistent

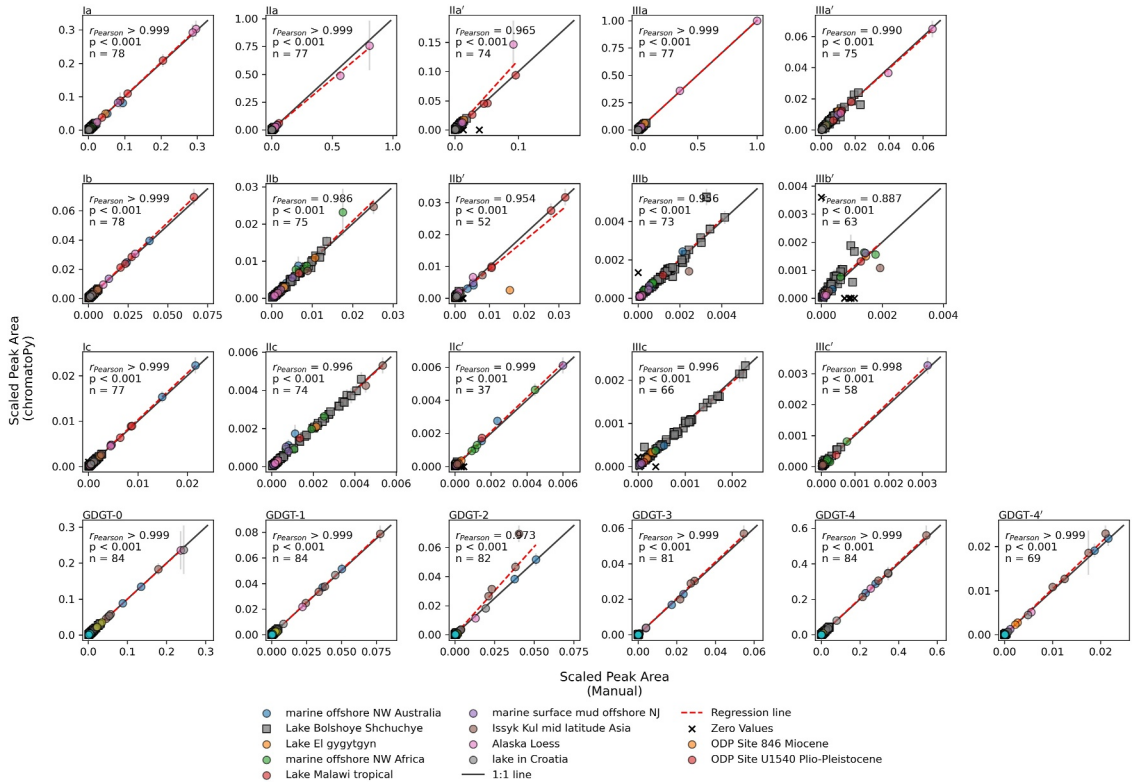

Figure 4. Comparison of scaled peak areas for individual Glycerol dialkyl glycerol tetraether structures using manual and chromatoPy integration.

with expectations from Gaussian deconvolution: the multi-Gaussian model can resolve and allocate more area to smaller, partially overlapping peaks that manual integration may under-represent, while proportionally reducing the area assigned to larger peaks. Similar systematic differences have been reported previously. For example, Fleming and Tierney (2016) found that a single-Gaussian model produced larger peak areas for brGDGTs relative to manual integration, while no differences were observed for isoGDGTs. Although our data set differs from that of Fleming and Tierney (2016), our results are consistent with the expectation that GDGTs less prone to co-elution, such as Ia, Ib, Ic, and GDGT-4, tend to yield slightly larger peak areas because they can be accurately represented by a single-Gaussian distribution. In contrast, compounds more affected by co-elution are deconvolved by chromatoPy's multi-Gaussian fitting algorithm, leading to a redistribution of peak area across overlapping peaks. This redistribution is illustrated in sample H1801000260 (Figure S2 in Supporting Information S1), which displays brGDGTs IIb′ and IIIb′ co-eluting with neighboring peaks. ChromatoPy's deconvolution assigns a greater proportion of area to these peaks, resulting in scaled peak areas that are 53.6% and 36.5% larger than their manually integrated replicates, respectively.

Although measurable, these differences have limited influence on more abundant compounds. For example, GDGT-4, GDGT-0, IIIa, and Ia remain virtually unaffected (Table 5). The most abundant GDGTs influenced by this bias are IIa and IIa′, which have median fractional abundances of 0.146 and 0.095, respectively. Yet the percent differences between methods for these compounds (−3.5% and 8.2%, respectively) translate to shifts of less than 0.01 in fractional abundance space. Thus, while the bias is detectable at the level of individual peak comparisons, its overall magnitude is small and unlikely to meaningfully affect downstream interpretations.

It is also important to note that direct comparisons between chromatoPy and manual integration are complicated by the inherent subjectivity of manual integration. In practice, peak truncation decisions vary between analysts and lack a predictable directional bias, whereas ChromatoPy applies a consistent, reproducible fitting procedure. Taken together, these results demonstrate that ChromatoPy provides highly comparable peak areas to manual integration, with systematic but minor differences for certain brGDGTs. The ability of ChromatoPy's multi-Gaussian fitting algorithm to objectively deconvolve co-eluting peaks underscores its utility for biomarker analysis.

Table 5
Wilcoxon Signed-Rank Test Results Comparing Fractional Differences Quantified With chromatoPy Versus Manual Integration

GDGT type	Wilcoxon Statistic	P-value	Median difference	Percent difference	Percent uncertainty
Ia	1,288	0.209	3.72E−04	0.247	1.54
Ib	1,081	0.022	1.87E−04	0.587	1.469
Ic	761	<0.001	1.52E−04	1.379	1.835
IIa	661	<0.001	−5.19E−03	−3.549	1.262
IIb	1,041	0.043	−6.91E−04	−1.356	2.389
IIc	1,278	0.438	−4.61E−05	−0.454	2.31
IIIa	799	<0.001	−1.50E−03	−0.458	1.549
IIIb	1,036	0.058	−1.59E−04	−0.857	1.947
IIIc	874	0.098	−6.56E−05	−0.75	2.161
IIa′	314	<0.001	7.85E−03	8.225	1.72
IIb′	271	<0.001	3.46E−03	16.687	2.757
IIc′	66	<0.001	8.75E−04	29.236	3.347
IIIa′	958	0.009	5.82E−03	6.356	2.428
IIIb′	296	<0.001	2.10E−03	25.742	4.431
IIIc′	224	<0.001	1.80E−04	9.201	3.008
GDGT-0	1,544	0.282	−5.43E−04	−0.144	0.814
GDGT-1	1,775	0.964	2.28E−04	0.369	1.496
GDGT-2	1,364	0.119	3.90E−04	1.328	2.521
GDGT-3	1,380	0.071	−2.42E−04	−3.494	2.203
GDGT-4	1,381	0.072	2.03E−03	0.392	0.679
GDGT-4′	886	0.041	−4.92E−04	−8.223	8.359

Note. Reported values also include the median difference, the median percent difference, and the absolute median percent uncertainty (calculated as the uncertainty relative to the chromatoPy-derived fractional abundance).

To assess whether these small differences in peak areas influence downstream proxies, we compare the temperature-sensitive methylation of branched tetraethers index (MBT'_{5Me}; De Jonge et al., 2014) for each sample (Figure 5). Across all samples, the median of differences between MBT'_{5Me} values is ∼0.004 with a 95th percentile range of −0.024 to 0.021. A Wilcoxon signed-rank test indicates that MBT'_{5Me} values calculated using peaks quantified via chromatoPy are significantly larger ($p < 0.001$) than those quantified using manual integration. This difference is consistent with Wilcoxon signed-rank tests of the fractional abundances of GDGTs quantified via the two integration methods. In comparison to the manual method, chromatoPy produces smaller fractional abundances of GDGTs in the denominator of the MBT'_{5Me} index (IIIa, IIIb, and IIIc), which would increase the resultant MBT'_{5Me} value.

While these results indicate a small but systematic offset in MBT'_{5Me} values, the magnitude of these differences remains minor. Importantly, the impact on MBT'_{5Me} falls well within the uncertainty bounds of published temperature calibrations. Using the slopes from four previously published temperature–MBT'_{5Me} calibration models, the translated median difference corresponds to at most 5.1% of the reported calibration uncertainty. We compared the RMSE values of these temperature–MBT'_{5Me} calibrations to the 1-σ standard deviation of the MBT'_{5Me} differences between manual and chromatoPy integration (Figure 4, Table 6), which represents at most 13.6% of the model uncertainties (Table 6; De Jonge et al., 2014; Naafs et al., 2017; Russell et al., 2018; Otiniano et al., 2023). The subtle differences between manual and chromatoPy-derived MBT'_{5Me} values are therefore unlikely to measurably influence climatic interpretations based on the GDGT proxy. This consistency reinforces the reliability of chromatoPy as an efficient and reproducible alternative to manual peak integration without compromising accuracy.

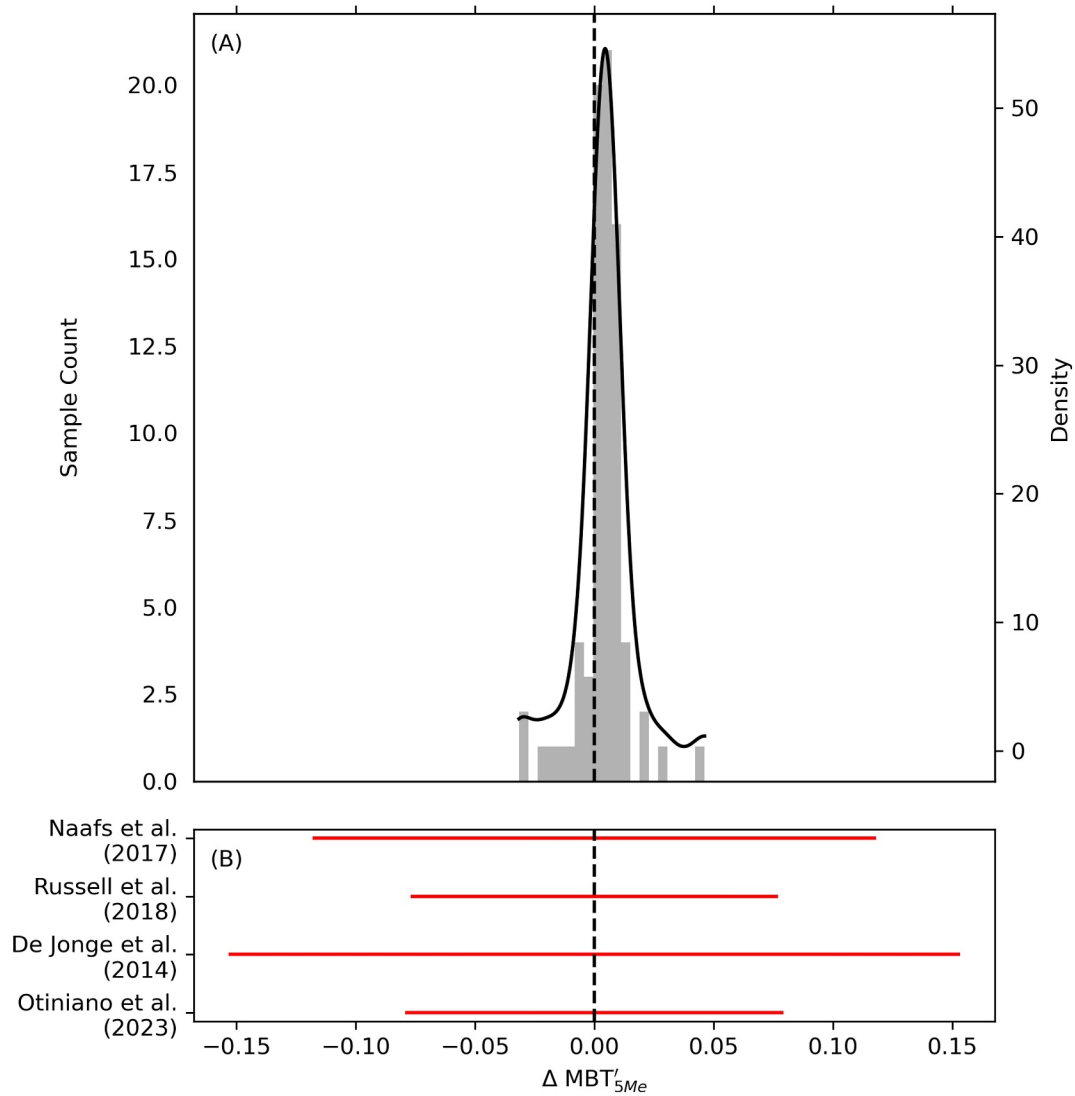

Figure 5. The impact of integration method on the MBT'_{5Me} index. (a) Histogram (gray bars) and Gaussian kernel density estimate (black line) of the residuals in MBT'_{5Me} ($\Delta MBT'_{5Me}$) between manual and chromatoPy integration. (b) Horizontal red bars show uncertainties of the temperature-MBT'_{5Me} calibration models, converted into MBT'_{5Me} space.

Table 6
Slopes and Associated Uncertainties From Published MBT'_{5Me}–Temperature Calibrations, With Corresponding References

Temperature - MBT'_{5Me} relationship (°C)	Uncertainty (°C)	Median translated temperature difference [1-σ] (°C)	Citation
40.01	4.7	0.15 [0.42]	Naafs et al. (2017)
32.42	2.47	0.12 [0.34]	Russell et al. (2018)
31.45	4.8	0.12 [0.33]	De Jonge et al. (2014)
14.75	1.16	0.06 [0.16]	Otiniano et al. (2023)

Note. These slopes were applied to differences in MBT'_{5Me} values derived from chromatoPy and manual integration methods, allowing calculation of the median and 1-σ temperature ranges.

3.4. Peak Area Uncertainty

ChromatoPy offers the first methodology that constrains some aspects of uncertainty when integrating GDGT peaks. In general, the uncertainties related to the Gaussian fitting parameters are low. When ranking peaks by their relative uncertainty, the 90th percentile range spans 0.8%–14.0% (Figure 3d–3f). In other words, the uncertainty band for a typical peak will represent only a small fraction of the integrated area. This generally low level of uncertainty also indicates that 1,000 iterations are sufficient for the multi-Gaussian fitting algorithm.

By contrast, the peaks with the highest relative uncertainty (i.e., above the 90th percentile) exhibit relative uncertainties ranging from 14.0% to 126.3%, consistent with a small subset of peaks that are either extremely small or poorly resolved (Figure 3d). These larger uncertainties are an important metric, identifying instances where chromatoPy's integration algorithm poorly fit a Gaussian model to the signal. In many cases, high relative uncertainty likely reflects attempts to integrate noisy data with low signal-to-noise ratios. Consistent with this interpretation, the median peak area of the upper 10% uncertainty group is only 163 amplitude•minutes, nearly an order of magnitude smaller than the median 1,410 amplitude•minutes observed for the lower 90%. In a few instances, peaks with large areas have high uncertainties. For peaks larger than 400 amplitude•minutes, 38 have relative uncertainties greater than 20%, and these generally are due to co-eluting iso- or brGDGTs. In such cases, chromatoPy can still provide an estimate of peak area, but improved chromatographic separation would reduce uncertainty. A separate source of large-peak uncertainty arises in highly concentrated samples, where peak distortion (e.g., fronting) compromises the assumed Gaussian peak shape. For example, the IIa peak from sample H2307066 has an associated relative uncertainty of ∼40%, which likely owes to fronting. High uncertainties should therefore be interpreted as a flag to re-examine the raw chromatogram and, if necessary, reprocess or reanalyze the sample.

3.5. Variance

Variance in peak areas provides a direct measure of the stability of peak integration and captures sources of variability beyond user decisions. In chromatoPy, uncertainty estimates already indicate that smaller peaks are subject to disproportionately higher variance relative to larger peaks (Figures 3a, 3b, and 3d). However, these uncertainties cannot fully account for the replicate differences observed among small peaks, pointing to an additional, un modeled source of variability. A similar size-dependent pattern appears when comparing chromatoPy and manual integrations of scaled peak areas, where smaller peaks show a wider array of percent differences relative to larger peaks (Figures 3f and 3g). This behavior is consistent with baseline noise, as baseline fluctuations constitute a minor fraction of larger peaks but grow in effect with smaller peaks. Because chromatoPy's present error budget includes only the Monte-Carlo spread of Gaussian fit parameters, baseline noise is effectively "missing" from the model. Therefore, incorporating a baseline term into the fitting algorithm, and therefore the parameter covariance matrix, would reduce the mismatch between algorithmic and empirical variance and will be incorporated in a future release of this product.

4. Conclusion

ChromatoPy offers a fast and effective method for the quantification of GDGTs measured via HPLC-MS. We developed our method assuming peak areas conform to a Gaussian distribution, thus facilitating integration via iterative fitting of Gaussian functions. We advance previous approaches by modeling multi-Gaussian functions that permit de-convolution of co-eluting peaks. This iterative curve-fitting approach also facilitates the first opportunity to systematically report GDGT peak area uncertainties. Although this approach does not yet capture all sources of uncertainty related to peak fitting, a future release of this package will improve on these methods without increasing the time required for processing, which is already an order of magnitude faster than manual integration.

Of particular importance, we establish standardized methods for baseline estimation and minimum peak amplitude thresholds, which will help improve comparability among analysts and laboratories. By combining deconvolution, quantified uncertainty, and standardized decision rules in an open-source package, chromatoPy enhances the reproducibility of GDGT quantification, an essential step toward more consistent proxy calibrations and the development of reliable, community-scale paleoclimate and biogeochemical data compilations. Building on this foundation, we will expand chromatoPy's capabilities to accommodate a wider range of chromatographic data, further establishing it as a robust, user-friendly tool for reproducible, high-throughput biomarker analysis.

Conflict of Interest

The authors declare no conflicts of interest relevant to this study.

Data Availability Statement

All raw and processed data, analysis outputs, and scripts used to generate figures and perform statistical analyses are available in a GitHub repository (https://github.com/GerardOtiniano/Otiniano-et-al.-chromatoPy-SI). A snapshot of this repository has been archived on Zenodo (Otiniano et al., 2025).

Acknowledgments
This research was supported by NSF Grants 1947981, 2044616, 2019652, and 2106971 to EKT. The authors thank Matthew Huber, editor for Paleoceanography and Paleoclimatology, as well as Fatemeh Ajallooeian and an anonymous reviewer for their constructive feedback that improved this manuscript.

References

Anderson, G. M. (1976). Error propagation by the Monte Carlo method in geochemical calculations. *Geochimica et Cosmochimica Acta*, *40*(12), 1533–1538. https://doi.org/10.1016/0016-7037(76)90092-2

Baxter, A. J., Hopmans, E. C., Russell, J. M., & Sinninghe Damsté, J. S. (2019). Bacterial GMGTs in East African lake sediments: Their potential as palaeotemperature indicators. *Geochimica et Cosmochimica Acta*, *259*, 155–169. https://doi.org/10.1016/j.gca.2019.05.039

Becker, K. W., Lipp, J. S., Versteegh, G. J. M., Wörmer, L., & Hinrichs, K.-U. (2015). Rapid and simultaneous analysis of three molecular sea surface temperature proxies and application to sediments from the Sea of Marmara. *Organic Geochemistry*, *85*, 42–53. https://doi.org/10.1016/j.orggeochem.2015.04.008

Chen, Y., Zheng, F., Yang, H., Yang, W., Wu, R., Liu, X., et al. (2022). The production of diverse brGDGTs by an Acidobacterium allows a direct test of temperature and pH controls on their distribution. *bioRxiv*. https://doi.org/10.1101/2022.04.07.487437

Currie, L. A. (1995). Nomenclature in evaluation of analytical methods including detection and quantification capabilities (IUPAC Recommendations 1995). *Pure and Applied Chemistry*, *67*(10), 1699–1723. https://doi.org/10.1351/pac199567101699

De Jonge, C., Hopmans, E. C., Stadnitskaia, A., Rijpstra, W. I. C., Hofland, R., Tegelaar, E., & Sinninghe Damsté, J. S. (2013). Identification of novel penta and hexamethylated branched glycerol dialkyl glycerol tetraethers in peat using HPLC–MS2, GC–MS and GC–SMB-MS. *Organic Geochemistry*, *54*, 78–82. https://doi.org/10.1016/j.orggeochem.2012.10.004

De Jonge, C., Hopmans, E. C., Zell, C. I., Kim, J.-H., Schouten, S., & Sinninghe Damsté, J. S. (2014). Occurrence and abundance of 6-methyl branched glycerol dialkyl glycerol tetraethers in soils: Implications for palaeoclimate reconstruction. *Geochimica et Cosmochimica Acta*, *141*, 97–112. https://doi.org/10.1016/j.gca.2014.06.013

De Jonge, C., Peterse, F., Nierop, K. G. J., Blattmann, T. M., Alexandre, M., Ansanay-Alex, S., et al. (2024). Interlaboratory comparison of branched GDGT temperature and pH proxies using soils and lipid extracts. *Geochemistry, Geophysics, Geosystems*, *25*(7), e2024GC011583. https://doi.org/10.1029/2024GC011583

Erb, D. (2024). Pybaselines: A Python library of algorithms for the baseline correction of experimental data. https://doi.org/10.5281/ZENODO.5608581

Felinger, A. (1994). Deconvolution of overlapping skewed peaks. *Analytical Chemistry*, *66*(19), 3066–3072. https://doi.org/10.1021/ac00091a013

Fleming, L. E., & Tierney, J. E. (2016). An automated method for the determination of the TEX86 and U37K′ paleotemperature indices. *Organic Geochemistry*, *92*, 84–91. https://doi.org/10.1016/j.orggeochem.2015.12.011

Haflidason, H., Brendryen, J., Eldegard, R. F., Mangerud, J., Olafsdottir, S., Regnéll, C., & Svendsen, J. I. (2022). High-resolution chronology of 24 000- year long cores from two lakes in the Polar Urals, Russia, correlated with palaeomagnetic inclination records with a distinct event about 20 000 years ago. *Journal of Quaternary Science*, *37*(5), 778–789. https://doi.org/10.1002/jqs.3391

Hopmans, E. C., Schouten, S., & Sinninghe Damsté, J. S. (2016). The effect of improved chromatography on GDGT-based palaeoproxies. *Organic Geochemistry*, *93*, 1–6. https://doi.org/10.1016/j.orggeochem.2015.12.006

Hopmans, E. C., Weijers, J. W. H., Schefuß, E., Herfort, L., Sinninghe Damsté, J. S., & Schouten, S. (2004). A novel proxy for terrestrial organic matter in sediments based on branched and isoprenoid tetraether lipids. *Earth and Planetary Science Letters*, *224*(1), 107–116. https://doi.org/10.1016/j.epsl.2004.05.012

Huguet, C., Hopmans, E. C., Febo-Ayala, W., Thompson, D. H., Sinninghe Damsté, J. S., & Schouten, S. (2006). An improved method to determine the absolute abundance of glycerol dibiphytanyl glycerol tetraether lipids. *Organic Geochemistry*, *37*(9), 1036–1041. https://doi.org/10.1016/j.orggeochem.2006.05.008

Johansson, M., Berglund, M., & Baxter, D. C. (1993). Improving accuracy in the quantitation of overlapping, asymmetric, chromatographie peaks by deconvolution: Theory and application to coupled gas chromatography atomic absorption spectrometry. *Spectrochimica Acta Part B: Atomic Spectroscopy*, *48*(11), 1393–1409. https://doi.org/10.1016/0584-8547(93)80127-G

Martínez-Sosa, P., & Tierney, J. E. (2019). Lacustrine brGDGT response to microcosm and mesocosm incubations. *Organic Geochemistry*, *127*, 12–22. https://doi.org/10.1016/j.orggeochem.2018.10.011

Mecozzi, M. (2014). A polynomial curve fitting method for baseline drift correction in the chromatographic analysis of hydrocarbons in environmental samples. *APCBEE Procedia*, *10*, 2–6. https://doi.org/10.1016/j.apcbee.2014.10.003

Naafs, B. D. A., Rohrssen, M., Inglis, G. N., Lähteenoja, O., Feakins, S. J., Collinson, M. E., et al. (2018). High temperatures in the terrestrial mid-latitudes during the early Palaeogene. *Nature Geoscience*, *11*(10), 766–771. https://doi.org/10.1038/s41561-018-0199-0

Naafs, B. D. A., Gallego-Sala, A. V., Inglis, G. N., & Pancost, R. D. (2017). Refining the global branched glycerol dialkyl glycerol tetraether (brGDGT) soil temperature calibration. *Organic Geochemistry*, *106*, 48–56. https://doi.org/10.1016/j.orggeochem.2017.01.009

Otiniano, G., Thomas, E., Castañeda, I., Acharya, S., & Mark, S. (2025). *GerardOtiniano/Otiniano-et-al.-chromatoPy-SI: V1.0 (Version V1.0). [Collection]*. Zenodo. https://doi.org/10.5281/ZENODO.16741093

Otiniano, G. A., Porter, T. J., Benowitz, J. A., Bindeman, I. N., Froese, D. G., Jensen, B. J. L., & Phillips, M. A. (2020). A late Miocene to late Pleistocene reconstruction of precipitation isotopes and climate from hydrated volcanic glass shards and biomarkers in central Alaska and Yukon. *Paleoceanography and Paleoclimatology*, *35*(7), e2019PA003791. https://doi.org/10.1029/2019PA003791

Otiniano, G. A., Porter, T. J., Buceta, R. E., Bergman, M. E., & Phillips, M. A. (2023). Climatic and environmentally driven variability in lacustrine brGDGT distributions at local to regional scales in Alaska and northwestern Canada. *Organic Geochemistry*, *181*, 104604. https://doi.org/10.1016/j.orggeochem.2023.104604

Patwardhan, A. P., & Thompson, D. H. (1999). Efficient synthesis of 40- and 48-Membered tetraether macrocyclic bisphosphocholines. *Organic Letters*, *1*(2), 241–244. https://doi.org/10.1021/ol990567o

Raberg, J. H., Harning, D. J., Crump, S. E., de Wet, G., Blumm, A., Kopf, S., et al. (2021). Revised fractional abundances and warm-season temperatures substantially improve brGDGT calibrations in lake sediments. *Biogeosciences*, *18*(12), 3579–3603. https://doi.org/10.5194/bg-18-3579-2021

Raberg, J. H., Miller, G. H., Geirsdóttir, A., & Sepulveda, J. (2022). Near-universal trends in brGDGT lipid distributions in nature. *Science Advances*, *8*(20), eabm7625. https://doi.org/10.1126/sciadv.abm7625

Rattray, J. E., & Smittenberg, R. H. (2020). Separation of Branched and Isoprenoid Glycerol Dialkyl Glycerol Tetraether (GDGT) isomers in peat soils and marine sediments using reverse phase chromatography. *Frontiers in Marine Science*, *7*, 539601. https://doi.org/10.3389/fmars.2020.539601

Russell, J. M., Hopmans, E. C., Loomis, S. E., Liang, J., & Sinninghe Damsté, J. S. (2018). Distributions of 5- and 6-methyl branched glycerol dialkyl glycerol tetraethers (brGDGTs) in East African lake sediment: Effects of temperature, pH, and new lacustrine paleotemperature calibrations. *Organic Geochemistry*, *117*, 56–69. https://doi.org/10.1016/j.orggeochem.2017.12.003

Savitzky, A., & Golay, M. J. E. (1964). Smoothing and differentiation of data by simplified least squares procedures. *Analytical Chemistry*, *36*(8), 1627–1639. https://doi.org/10.1021/ac60214a047

Schmid, M., Rath, D., & Diebold, U. (2022). Why and how savitzky–golay filters should be replaced. *ACS Measurement Science Au*, *2*(2), 185–196. https://doi.org/10.1021/acsmeasuresciau.1c00054

Schneider, T., Castañeda, I. S., Zhao, B., Krüger, S., Salacup, J. M., & Bradley, R. S. (2024). Tracing Holocene temperatures and human impact in a Greenlandic Lake: Novel insights from hyperspectral imaging and lipid biomarkers. *Quaternary Science Reviews*, *339*, 108851. https://doi.org/10.1016/j.quascirev.2024.108851

Schouten, S., Forster, A., Panoto, F. E., & Sinninghe Damsté, J. S. (2007). Towards calibration of the TEX86 paleothermometry for tropical sea surface temperatures in ancient greenhouse worlds. *Organic Geochemistry*, *38*(9), 1537–1546. https://doi.org/10.1016/j.orggeochem.2007.05.014

Schouten, S., Hopmans, E. C., Schefuß, E., & Sinninghe Damsté, J. S. (2002). Distributional variations in marine crenarchaeotal membrane lipids: A new tool for reconstructing ancient sea water temperatures? *Earth and Planetary Science Letters*, *204*(1), 265–274. https://doi.org/10.1016/S0012-821X(02)00979-2

Sinninghe Damsté, J. S., Rijpstra, W. I. C., Hopmans, E. C., Weijers, J. W., Foesel, B. U., Overmann, J., & Dedysh, S. N. (2011). 13,16-Dimethyl octadecanedioic acid (iso-Diabolic acid), a common membrane-spanning lipid of acidobacteria subdivisions 1 and 3. *Applied and Environmental Microbiology*, *77*(12), 4147–4154. https://doi.org/10.1128/AEM.00466-11

Vemula, H., Kitase, Y., Ayon, N. J., Bonewald, L., & Gutheil, W. G. (2017). Gaussian and linear deconvolution of LC-MS/MS chromatograms of the eight aminobutyric acid isomers. *Analytical Biochemistry*, *516*, 75–85. https://doi.org/10.1016/j.ab.2016.10.017

Virtanen, P., Gommers, R., Oliphant, T. E., Haberland, M., Reddy, T., Cournapeau, D., et al. (2020). SciPy 1.0: Fundamental algorithms for scientific computing in Python. *Nature Methods*, *17*(3), 261–272. https://doi.org/10.1038/s41592-019-0686-2

Wei, X., Shi, X., Kim, S., Patrick, J. S., Binkley, J., Kong, M., & Zhang, X. (2014). Data dependent peak model based spectrum deconvolution for analysis of high resolution LC-MS data. *Analytical Chemistry*, *86*(4), 2156–2165. https://doi.org/10.1021/ac403803a

Weijers, J. W., Schouten, S., Hopmans, E. C., Geenevasen, J. A. J., David, O. R. P., Coleman, J. M., et al. (2006). Membrane lipids of mesophilic anaerobic bacteria thriving in peats have typical archaeal traits. *Environmental Microbiology*, *8*(4), 648–657. https://doi.org/10.1111/j.1462-2920.2005.00941.x

Yao, Y., Zhao, J., Vachula, R. S., Werne, J. P., Wu, J., Song, X., & Huang, Y. (2020). Correlation between the ratio of 5-methyl hexamethylated to pentamethylated branched GDGTs (HP5) and water depth reflects redox variations in stratified lakes. *Organic Geochemistry*, *147*, 104076. https://doi.org/10.1016/j.orggeochem.2020.104076

Yu, T., & Peng, H. (2010). Quantification and deconvolution of asymmetric LC-MS peaks using the bi-Gaussian mixture model and statistical model selection. *BMC Bioinformatics*, *11*(1), 559. https://doi.org/10.1186/1471-2105-11-559

Zeng, Z., Chen, H., Yang, H., Chen, Y., Yang, W., Feng, X., & Welander, P. V. (2022). Identification of a protein responsible for the synthesis of archaeal membrane-spanning GDGT lipids. *Nature Communications*, *13*(1), 1545. https://doi.org/10.1038/s41467-022-29264-x

Zhang, Z., Smittenberg, R. H., & Bradley, R. S. (2016). GDGT distribution in a stratified lake and implications for the application of TEX86 in paleoenvironmental reconstructions. *Scientific Reports*, *6*(1), 34465. https://doi.org/10.1038/srep34465